BRL

MEMORANDUM REPORT NO. 2770

TEMPERATURE MEASUREMENT OF RESIDUAL PENETRATION FRAGMENTS

W. G. Von Holle
G. Melani
J. Waddell
R. Frey

July 1977

USA ARMAMENT RESEARCH AND DEVELOPMENT COMMAND
USA BALLISTIC RESEARCH LABORATORY
ABERDEEN PROVING GROUND, MARYLAND

Destroy this report when it is no longer needed.
Do not return it to the originator.

Secondary distribution of this report by originating or sponsoring activity is prohibited.

Additional copies of this report may be obtained from the National Technical Information Service, U.S. Department of Commerce, Springfield, Virginia 22151.

The findings in this report are not to be construed as an official Department of the Army position, unless so designated by other authorized documents.

The use of trade names or manufacturers' names in this report does not constitute indorsement of any commercial product.

UNCLASSIFIED

SECURITY CLASSIFICATION OF THIS PAGE *(When Data Entered)*

REPORT DOCUMENTATION PAGE

READ INSTRUCTIONS BEFORE COMPLETING FORM

1. REPORT NUMBER: BRL Memorandum Report No. 2770	2. GOVT ACCESSION NO.
3. RECIPIENT'S CATALOG NUMBER	
4. TITLE *(and Subtitle)*: TEMPERATURE MEASUREMENT OF RESIDUAL PENETRATION FRAGMENTS	5. TYPE OF REPORT & PERIOD COVERED
	6. PERFORMING ORG. REPORT NUMBER
7. AUTHOR(s): W. G. Von Holle, G. Melani, J. Waddell, R. Frey	8. CONTRACT OR GRANT NUMBER(s)
9. PERFORMING ORGANIZATION NAME AND ADDRESS: US Army Ballistic Research Laboratory, Aberdeen Proving Ground, MD 21005	10. PROGRAM ELEMENT, PROJECT, TASK AREA & WORK UNIT NUMBERS: 1L662618AH80
11. CONTROLLING OFFICE NAME AND ADDRESS: US Army Materiel Development & Readiness Command, 5001 Eisenhower Avenue, Alexandria, VA 22333	12. REPORT DATE: JULY 1977
	13. NUMBER OF PAGES: 38
14. MONITORING AGENCY NAME & ADDRESS *(if different from Controlling Office)*	15. SECURITY CLASS. *(of this report)*: UNCLASSIFIED
	15a. DECLASSIFICATION/DOWNGRADING SCHEDULE

16. DISTRIBUTION STATEMENT *(of this Report)*

Approved for public release; distribution unlimited.

17. DISTRIBUTION STATEMENT *(of the abstract entered in Block 20, if different from Report)*

18. SUPPLEMENTARY NOTES

19. KEY WORDS *(Continue on reverse side if necessary and identify by block number)*

Temperature
Fragments
Radiometry
Infrared
Penetration

20. ABSTRACT *(Continue on reverse side if necessary and identify by block number)* (klb)

The temperature of residual fragments from the low velocity penetration of 1.27 steel spheres into various targets has been measured by 2-band infrared radiometry. The residual velocities of the fragments were also measured. The temperatures correlate well with the predictions of a simple model based on the conversion of mechanical energy to heat. The residual velocities correlate with theoretical and previous empirical data.

DD FORM 1 JAN 73 1473 EDITION OF 1 NOV 65 IS OBSOLETE

UNCLASSIFIED

SECURITY CLASSIFICATION OF THIS PAGE *(When Data Entered)*

TABLE OF CONTENTS

LIST OF ILLUSTRATIONS

LIST OF TABLES

I. INTRODUCTION

Many data have been published on residual fragment diagnostics from penetration of simple projectiles. However, no temperature measurements have been reported. The purpose of this study is to measure the temperature of such fragments in flight using the new technique of two-color infrared radiometry, which has been recently applied to the study of shocked copper plates and shaped charge jets in free flight[1,2,3]. Briefly, the two-color radiometric technique eliminates the inherent deficiencies of the "brightness" or single-band method by the cancellation of emittance and geometrical errors. This is accomplished by the measurement of the radiance ratio in two closely spaced wavelength bands originating from the same surface area.

Knowledge of the temperature of residual fragments as a function of projectile impact velocity and target thickness is important in its own right, but the present investigation is designed mainly to support the study of fragment initiation of confined explosives and propellants. The temperature of the resulting fragments from such penetrations is of paramount importance in deciding on an initiation mechanism for a given situation. Shock initiation may be the dominant mechanism at high impact velocities and light confinement while heat conduction from a hot fragment may become important at lower velocities and thicker barriers.

II. EXPERIMENTAL

Steel spheres of 1.27 cm (0.5 inch) diameter were fired from a conventional powder gun at mild steel targets of 3.2 mm (1/8 inch), 6.3 mm (1/4 inch), and 12.7 mm (1/2 inch) thickness at a 5 meter range. Impact velocities ranged from 0.405 mm/μsec to 1.558 mm/μsec.

The radiometers viewed the residual fragments in air at points located from 31.8 mm (1 1/4 inch) to 63.5 mm (2 1/2 inch) from the rear surface of the target on the normal path of the projectile. The line drawing of Figure 1 shows the arrangement. At a range of 1.3 meters the spot size of each radiometer was about four millimeters square. The

---

[1] *W. G. Von Holle and J. J. Trimble, "Residual Temperature of Shocked Solids by Two-Band Infrared Radiometry," BRL Report MR2624, May 1976.* (AD #B011450L)

[2] *W. G. Von Holle and J. J. Trimble, "Temperature Measure of Shocked Copper Plates and Shaped Charge Jets by Two-Color I. R. Radiometry," J. Appl. Phys., 47, 2391 (1976).*

[3] *W. G. Von Holle and J. J. Trimble, "Shaped Charge Temperature Measurement," Proceedings of the Sixth Symposium on Detonation, San Diego, California, August 1976.*

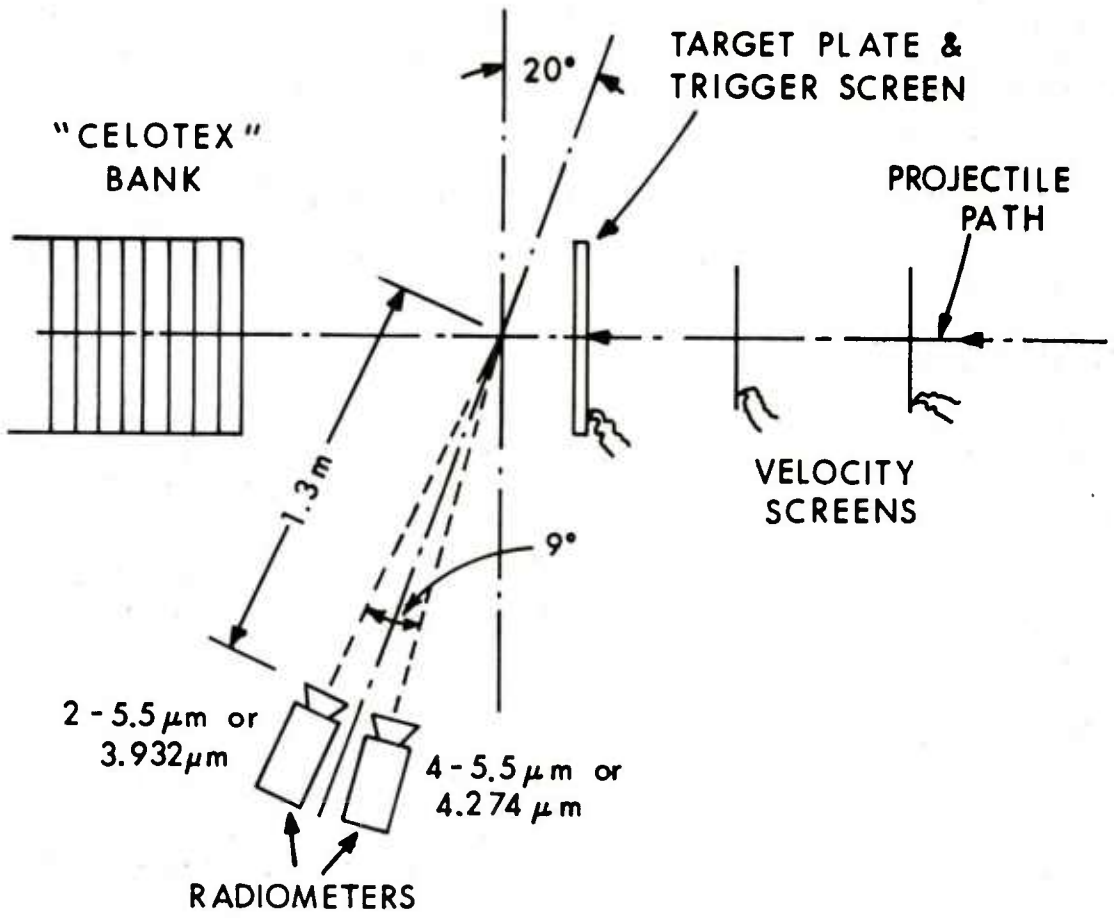

Figure 1. Schematic drawing of the experimental arrangement used for obtaining residual fragment temperatures.

radiometers were aligned and focused by means of a small loop of heated Nichrome wire. Radiometer signal voltage versus time data were obtained by a single oscilloscope chopped between the two radiometer output signals or by a scope for each radiometer. Time sweeps were triggered by conventional printed "make" screens taped to the front of the target plate.

The radiometers were calibrated with a mild steel surface polished with 600 grit paper and heated in vacuum in an induction furnace according to a previously described procedure[3]. Results of this calibration for the 3.938 μm/4.274 μm ratio and the broad-band ratio are shown in Figures 2 and 3.

III. RESULTS

A. 12.7 mm Targets

Figure 4 shows a typical trace of the radiance signals chopped between the broad-band radiometer outputs of shot#862. In this instance two major fragments were recovered in fibre-board behind the event. The impacting projectile, which had been flattened, and a large portion of the plug were found in the recovery medium, separated, but in close proximity. The first component of the large split peak was thus assigned to the plug and the second to the ball. Much more complicated traces were obtained from hard, unannealed spheres which were used initially and then abandoned in favor of the soft, annealed projectiles. The radiographs of Figure 5 show soft and hard spheres after penetration of 12.7 mm targets. The hard metal breaks up into many small pieces while the soft ball merely becomes distorted. Figure 6 is a photograph of representative recovered fragments from shots with all three target thicknesses. It was concluded from examination of the recovered fragments of this program that most penetrations took place by a plugging mechanism.

The plug and ball seldom followed the same path unless they were stuck together. The ball usually deviated more from the path normal to the target allowing only the plug to pass the radiometers field-of-view. Figure 4 shows traces from such a shot, #901, in which only the plug radiance is prominant. Most of the data on the 12.7 mm targets are for the plug. Table I lists the results for 12.7 mm target plate. Up to three radiance maxima occur in the records. T_1, T_2, and T_3 are the temperatures derived from the radiance ratios of the first, second, and third peaks, respectively. T_1 is the plug temperatures. T_2 has been tenatively assigned to be the ball temperature, and T_3 is believed to be due to debris. These assignments of temperature are the most reasonable interpretation of the data. Figure 7 is a plot of T_1, (plug temperature) versus impact velocity. Only shots #861 and 862 provided the possibility of ball temperature measurement.

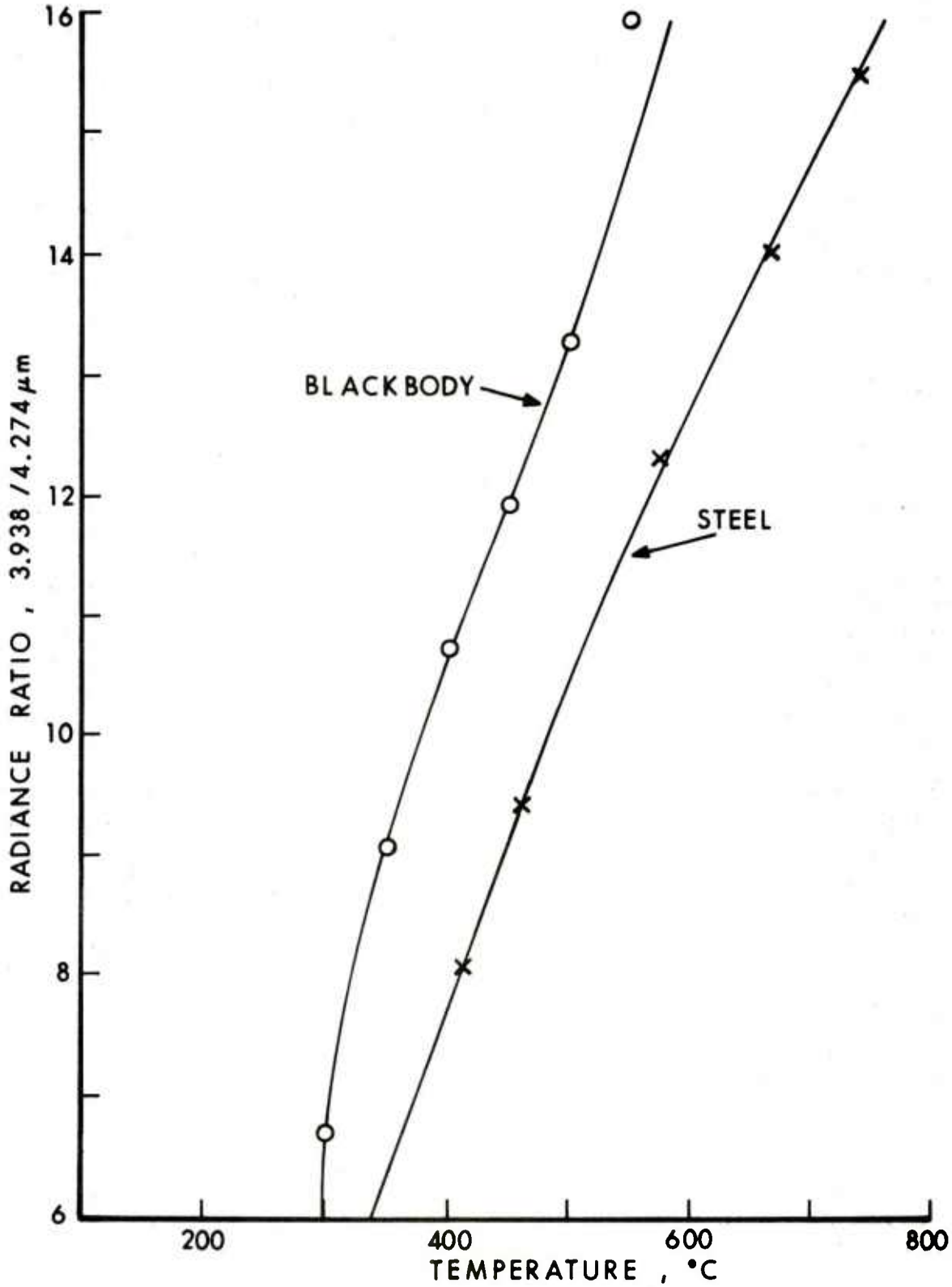

Figure 2. Calibration curves for steel and a blackbody source obtained with the broad-band radiometers, 2-5.5 μm and 4-5.5 μm.

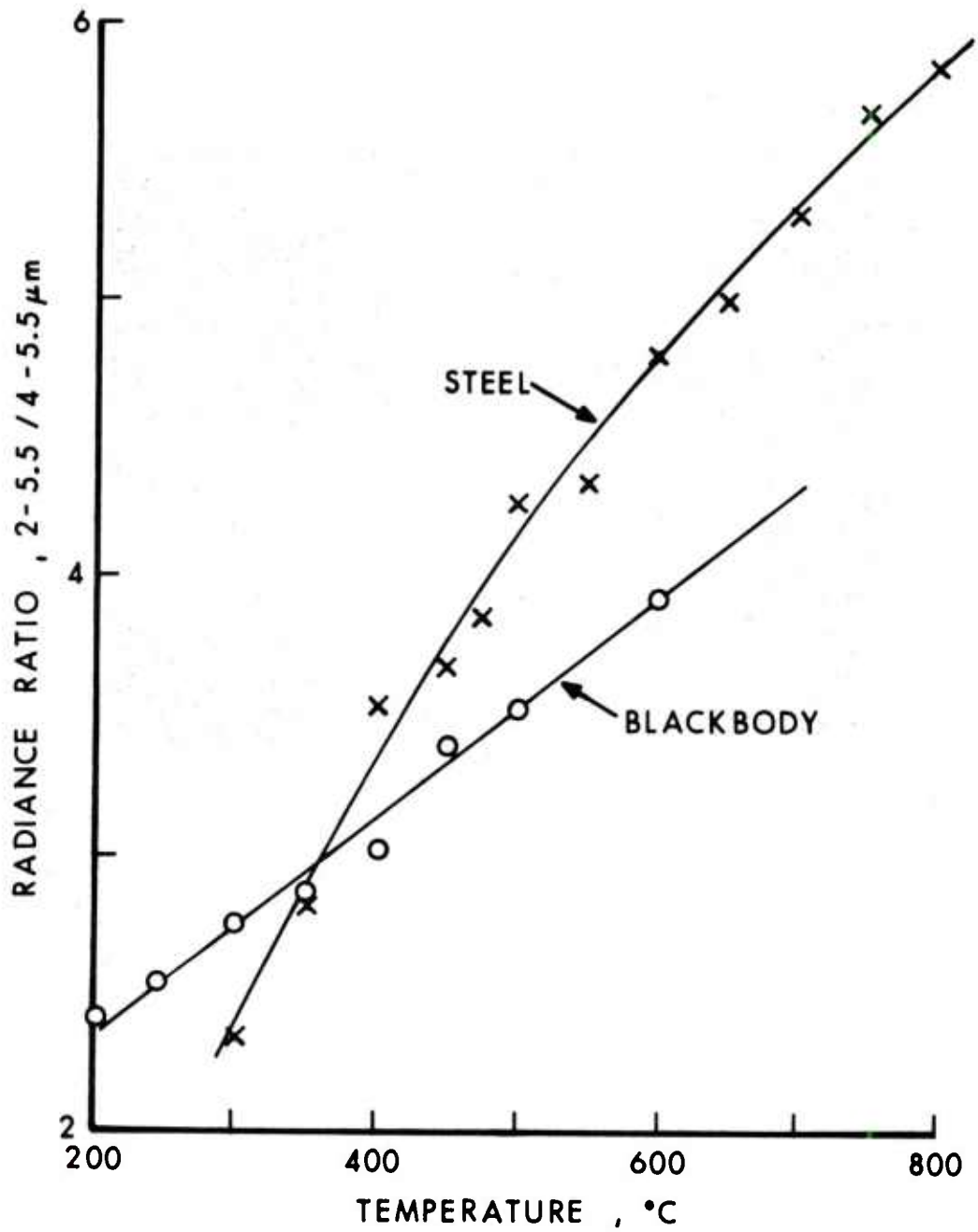

Figure 3. Calibration curves for steel and a blackbody source obtained with the narrow-band filters, 3.938 µm and 4.274 µm.

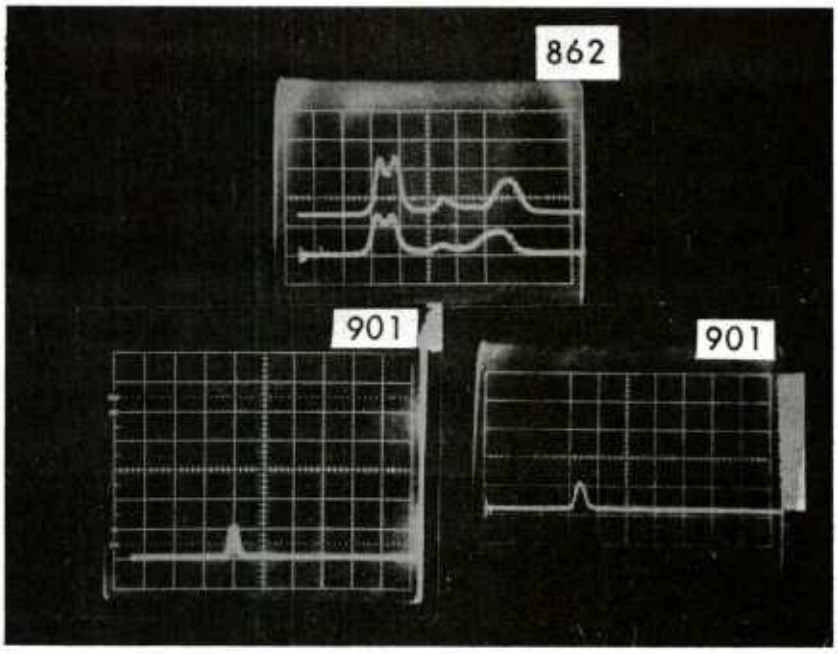

Figure 4. Typical oscilloscope traces obtained from penetration of 12.7 mm targets. Shot #862 was obtained from chopped input signal, the upper trace is the 3.938 μm signal at 500 mV/div.; the lower is the 4.274μm output at 50 mV/div. Shot #901 was run at the same sensitivities and sweep rate with two separate scopes; the left trace is the 3.938 μm signal and the right one is the 4.274 μm signal.

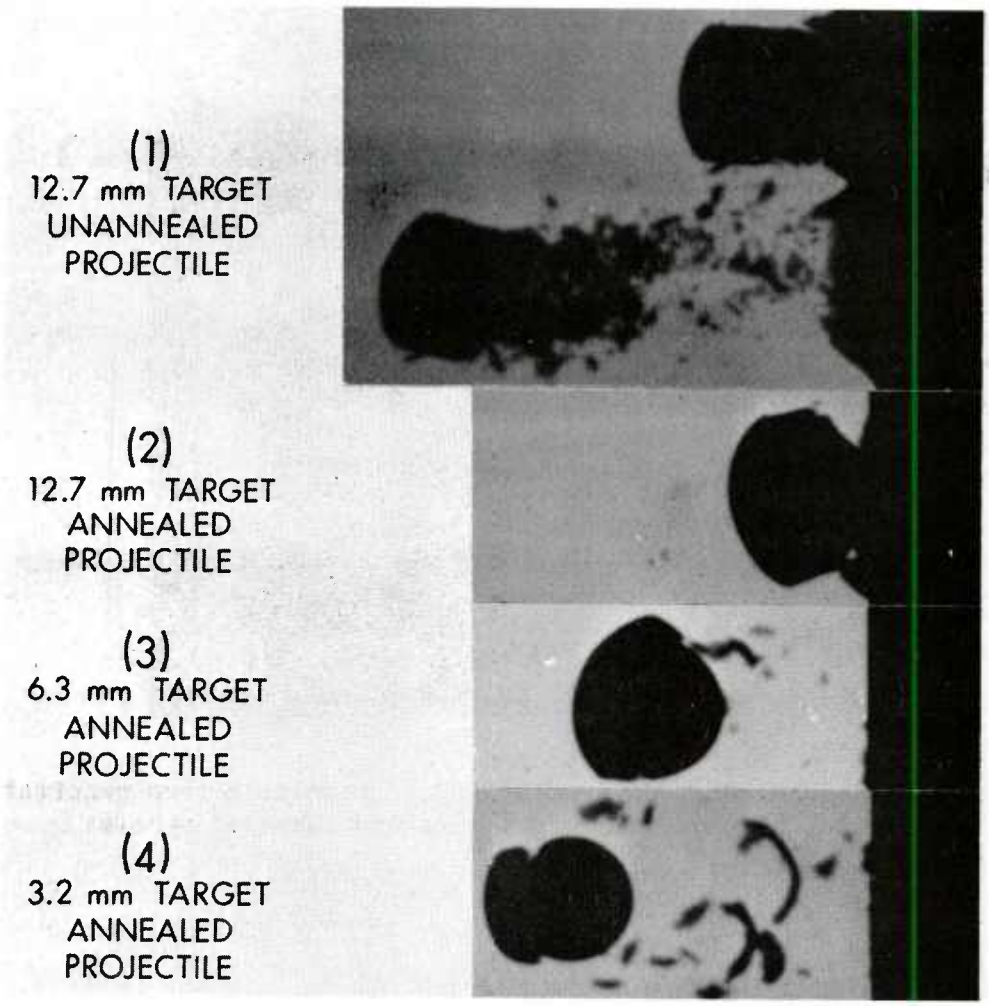

Figure 5. Radiographs of the 1.27 cm projectile penetration for the three targets used in this report. The first is a double exposure separated by 210μs with unannealed projectiles on 12.7 mm targets; impact velocity is 1.21 mm/μs. The second is an annealed projectile with the same target; the velocity is 1.40 mm/μs. The next is a 6.3 mm target at 0.92 mm/μs and the last a 3.2 mm target at 0.78 mm/μs. The x-rays were triggered at various times after impact. The magnification is 1.28.

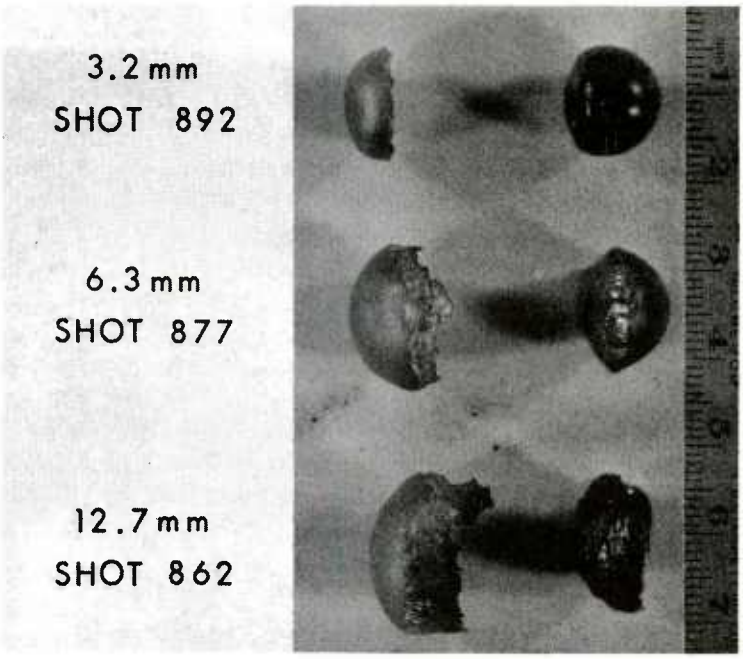

Figure 6. Photograph of recovered fragments resulting from penetration of the three targets by the 1.27 cm annealed spheres.

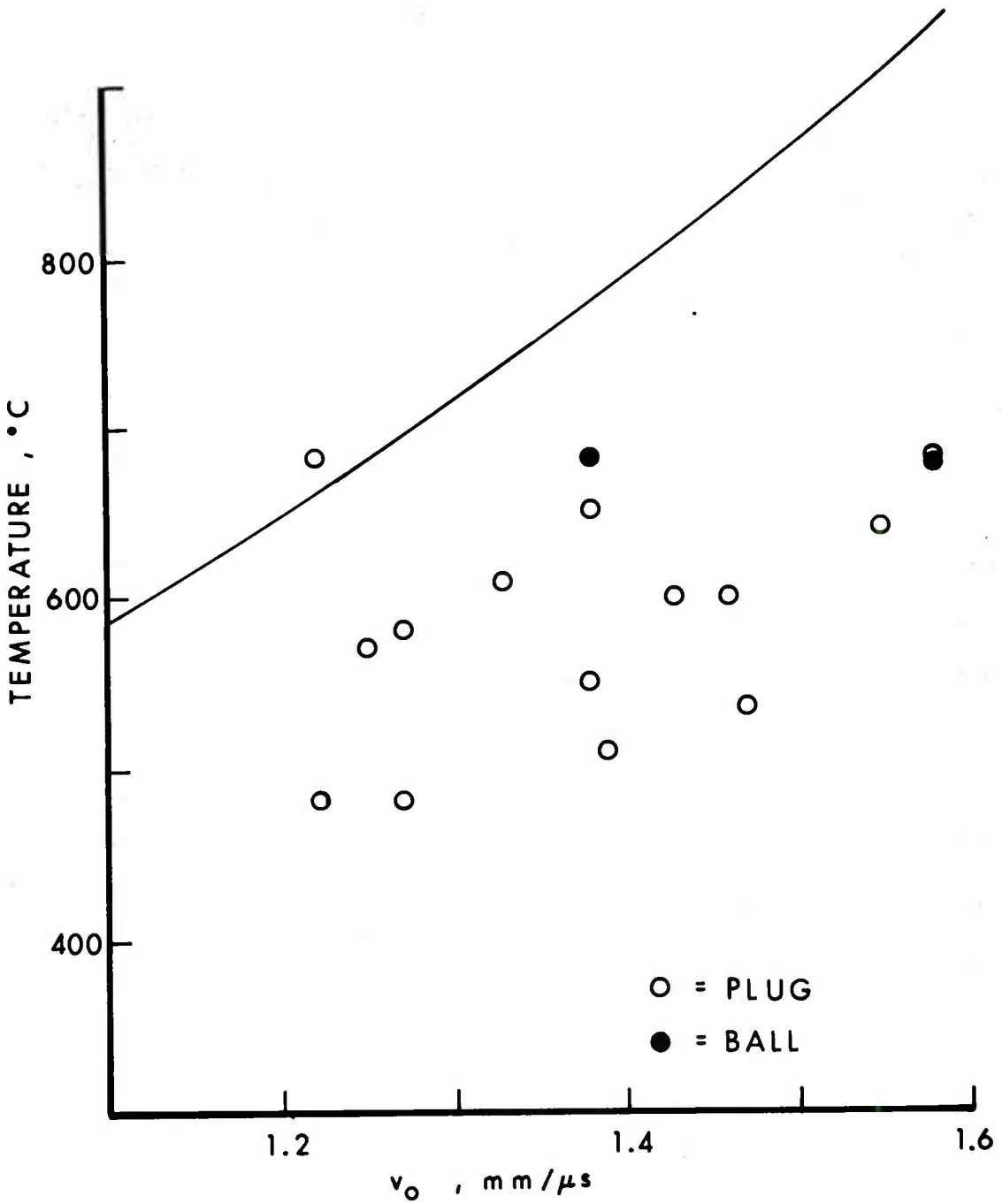

Figure 7. Plot of experimental results for the 12.7 μs target. Most plug results were obtained with unannealed projectiles. The solid curve is the temperature predicted from the model.

Table I. 12.7 mm Target Data

Shot #	v_o (mm/μs)	T_1 (°C)	T_2 (°C)	T_3 (°C)	Projectile (H=hard, A=annealed)
821	1.27	-	580	690	H
822	1.25	570	575	470	H
823	1.22	680	630	610	H
836	1.27	480	670	-	H
837	1.47	-	535	-	H
846	1.22	480	-	-	H
847	1.43	-	600	550	H
858	1.33	610	600	485	H
859	1.38	550	540	-	
860	1.55	640	680	555	H
901	1.39	510	-	-	A
861	1.58	680	680	340	A
862	1.38	650	680	-	A
902	1.46	600	-	-	A

B. 6.3 mm Targets

The 6.3 mm targets provided the most complicated and most difficult traces to interpret even with the use of annealed projectiles. Traces from three representative shots are presented in Figure 8. At low impact velocities such as in shot#882, the fragments and plug were recovered in contact with one another. This indicates that they were close together as they passed by the radiometers, yielding infrared signal traces dominated by a single broad peak with only weak shoulders. As the velocity is increased as in shots 877 and 875 considerable structure appears in the traces, and the plug and residual sphere were not in contact when recovered. Also, in all cases of high velocity, many smaller pieces of plug are formed which may or may not cross the field-of-view of the radiometers. The radiograph of Figure 5 for the 6.3 mm plate clearly shows the separation of plug and ball as well as some debris.

Table II shows all 6.3 mm target results with the temperatures derived for the first three radiance peaks where measurable. Figure 9 is a plot of temperature data versus impact velocity. T_1, which is due to the plug, is plotted separately from T_3, which is assigned to the ball temperature. T_2 occurs very close to T_1 and is also assigned to the plug. The fact that the plug can be resolved into two peaks is made believable by examination of the recovered fragments which show the two regions of the plug (see Figure 6). The first (T_1) is a result of the bulge of the plate and second (T_2) the sheared part. Not all signal traces show good resolution of these two features. Either T_1 or T_2 was plotted in Figure 9 depending on signal strength and resolution of the peak. T_3 was always assigned to the residual sphere.

C. 3.2 mm Target

Although only a few shots were fired, the signal intensities and the temperatures show more regularity for this target than the others. Traces for two extremes of impact velocity are presented in Figure 10. In shot#890, the signal level is very low but structure can be discerned. In #893, the radiances are much greater. The first peak may be due to ejecta from the surface caused by the strong shock induced in the thin target plate. The fact that this first radiance peak increases in intensity very rapidly with impact velocity while the ratio (temperature) remains low seems to support this assignment. An optically thin object could increase in radiance without a concomitant temperature rise if its thickness increased. For an optically thin layer of material, the radiance is proportional to the product of the thickness and the absorption coefficient. Thus, a small increase in this product will cancel out in the radiance ratio, assuming the absorption coefficient does not vary appreciably over the wavelength range of the 2-color radiometer.

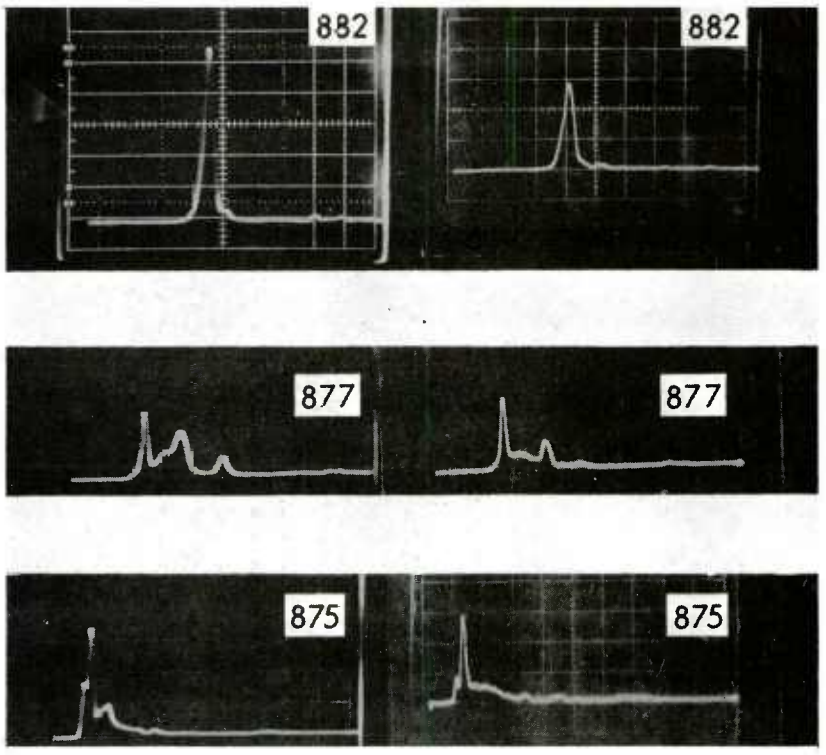

Figure 8. Typical oscilloscope traces obtained from 6.3 mm targets. The first set, on top, is Shot #882; 2-5.5 μm, at 200 mV/div. on the left and the 4-5.5 μm trace on the right at 100 mV/div. In the middle, Shot #877, the 2-5.5 μm trace was run at 500 mV/div. and the 4-5.5 μm trace at 200 mV/div. Shot #875 is last with the 3.938 μm trace on the left at 500 mV/div. and the 4.274 μm trace on the right at 50 mV/div. Each trace was swept at 50 μsec.

Table II. 6.3 mm Target Data

Shot #	v_o (mm/μs)	T_1(°C)	T_2(°C)	T_3(°C)	Projectile (H=hard, A=annealed)
864	1.28	510	690	680	H
865	1.25	-	480	495	H
868	1.24	-	480	420	A
871	1.28	730	-	405	A
873	1.25	650	550	550	A
874	1.22	-	545	435	A
875	1.49	800	535	585	A
876	1.11	310	-	-	A
877	0.967	290	600	415	A
878	0.810	540	-	-	A
879	0.764	485	-	-	A
882	0.776	440	-	-	A
895	1.15	380	440	310	A
896	1.03	315	400	325	A
897	1.05	-	420	310	A
908	0.868	265	360	200	A

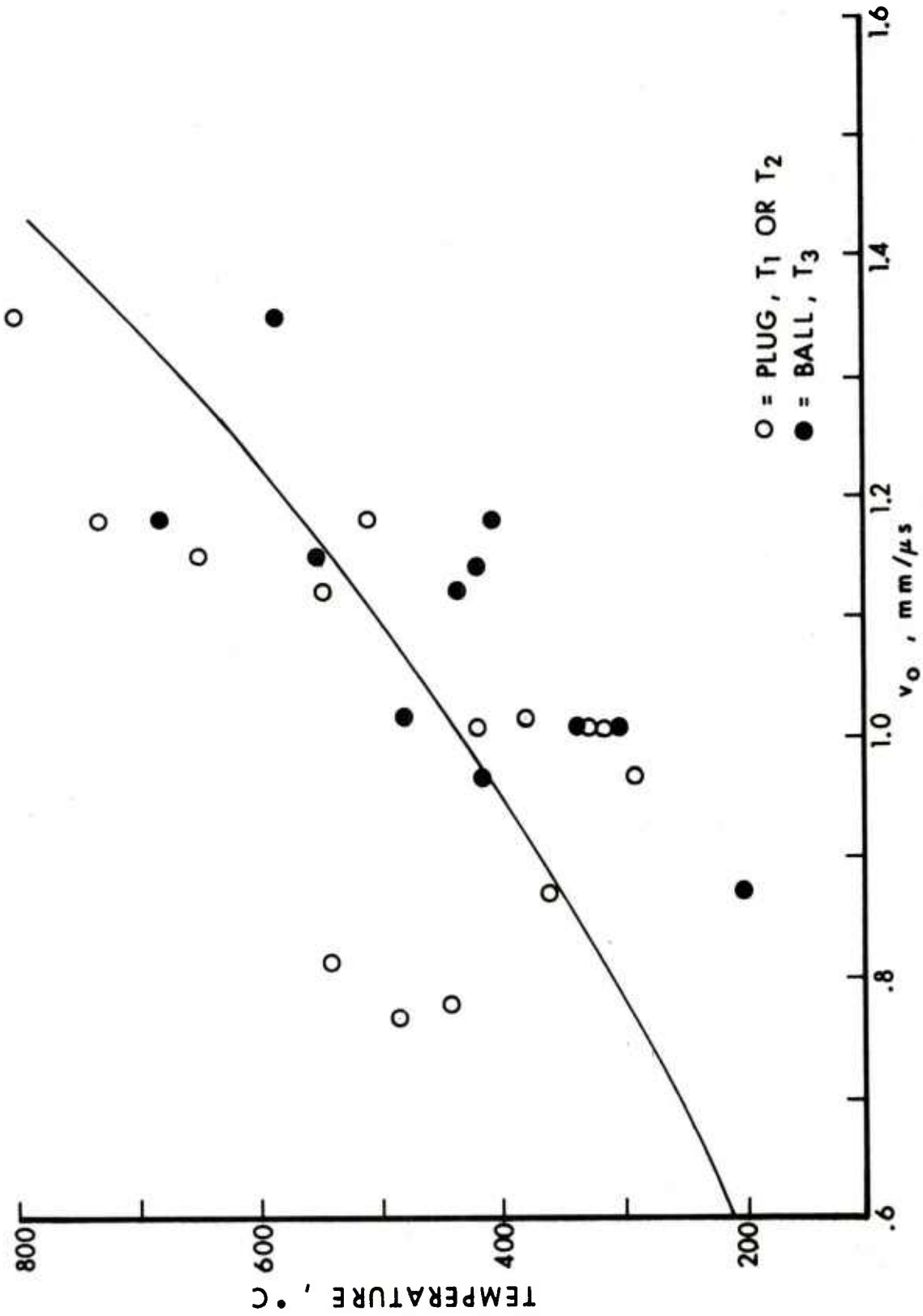

Figure 9. Plot of experimental results for the 6.3 mm target. The solid curve is the temperature predicted from the model.

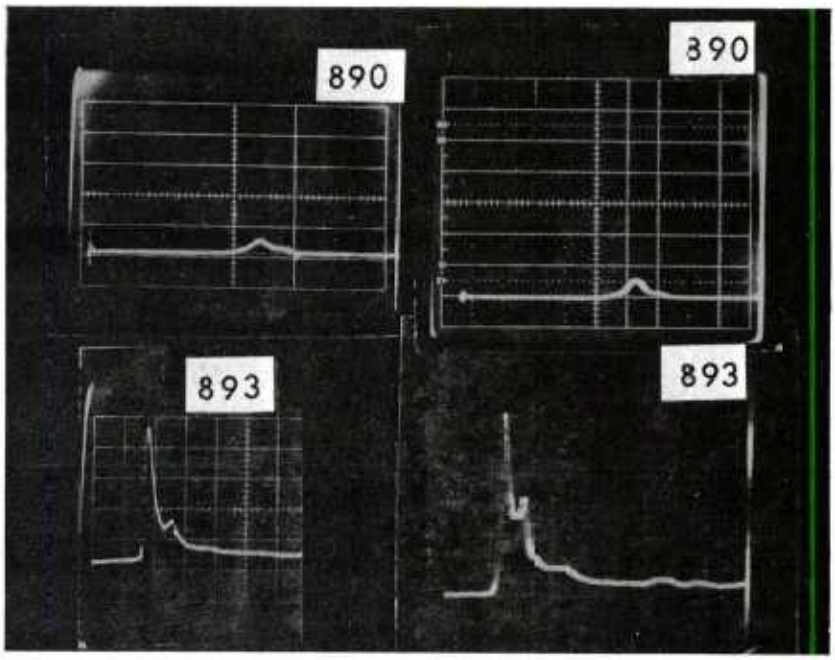

Figure 10. Typical oscilloscope traces obtained from 3.2 mm targets. The top two traces are from Shot #890; the 4-5.5 μm output is on the left at 100 mV/div and the 2-5.5 μm output on the right at 200 mV/div. The two lower traces are from Shot #893; the one on the left is the 4-5.5 μm trace at 50 mV/div. and the 2-5.5 μm trace is on the right at 100 mV/div. Each time sweep was 50 μs/div.

Table III. 3.2 mm Target Data

Shot #	v_o (mm/μs)	T_1(°C)	T_2(°C)	T_3(°C)
890	0.405	-	340	250
891	0.603	465	295	-
892	0.657	275	465	340
893	0.738	325	605	360
894	0.800	320	770	365

Table III shows the results for the 3.2 mm targets. T_1 and T_3 remain relatively unchanged as T_2 increases rapidly with impact velocity. Figure 11 shows a plot of residual fragment temperatures versus impact velocity for the 3.2 mm targets.

D. Projectile before Impact

Several shots were fired without target plates in order to measure the effect of gun-launch and aerodynamic heating on the projectile temperature. Table IV lists the results of all of these firings, including those obtained from the use of sabots to fire the 1.27 cm spheres, eliminating the effect of barrel friction. Each of the radiance peaks were multiple, and, when the oscilloscopes were triggered with the trigger screen close to the observation point, the radiance signal levels were higher. This may indicate that a spray of paper particles caused the additional peaks, interfering with the observation. (The effect of the velocity screen on the front of the steel target is expected to be small.) If one considers only the cases where the trigger was relatively far away (85.7 and 400 mm), the difference between saboted and unsaboted spheres is small. Thus the measured temperature is probably caused by aerodynamic heating, which would not be expected to affect significantly the temperature measurements of the target plate residual fragments since they are traveling much slower than the impact velocities. Also, the air shock wave would not be expected to interfere in the target shots, except perhaps with the 3.2 mm plate shots, because the residual velocity is low. Such transient heating effects would be expected to heat only the first few atomic layers of the projectile and to equilibrate quickly.

E. Residual Velocities

Residual velocities for first fragments to arrive at the focal point (plugs) and residual spheres were calculated and plotted against the impact velocities in Figures 12, 13 and 14. The experimental residual velocities, v_R, were computed by dividing the distance from target plate to the radiometer focal point by the time from scope trigger to the particular feature of interest as read from the oscilloscope traces. The reason for this exercise is merely to provide a check on the credibility of the infrared data. Admittedly, the uncertainty in these residual velocities is much greater than those obtained with velocity screens. (However, this method does measure velocities of different particles on the same shot.) Two residual velocity curves are included for each case for comparison. An expression for residual velocity for plugging due to Recht[4] is given in equation (1) and plotted

[4] *R. F. Recht and T. W. Ipson, "Ballistic Perforation Dynamics," J. Appl. Mech., 30, 384 (1963).*

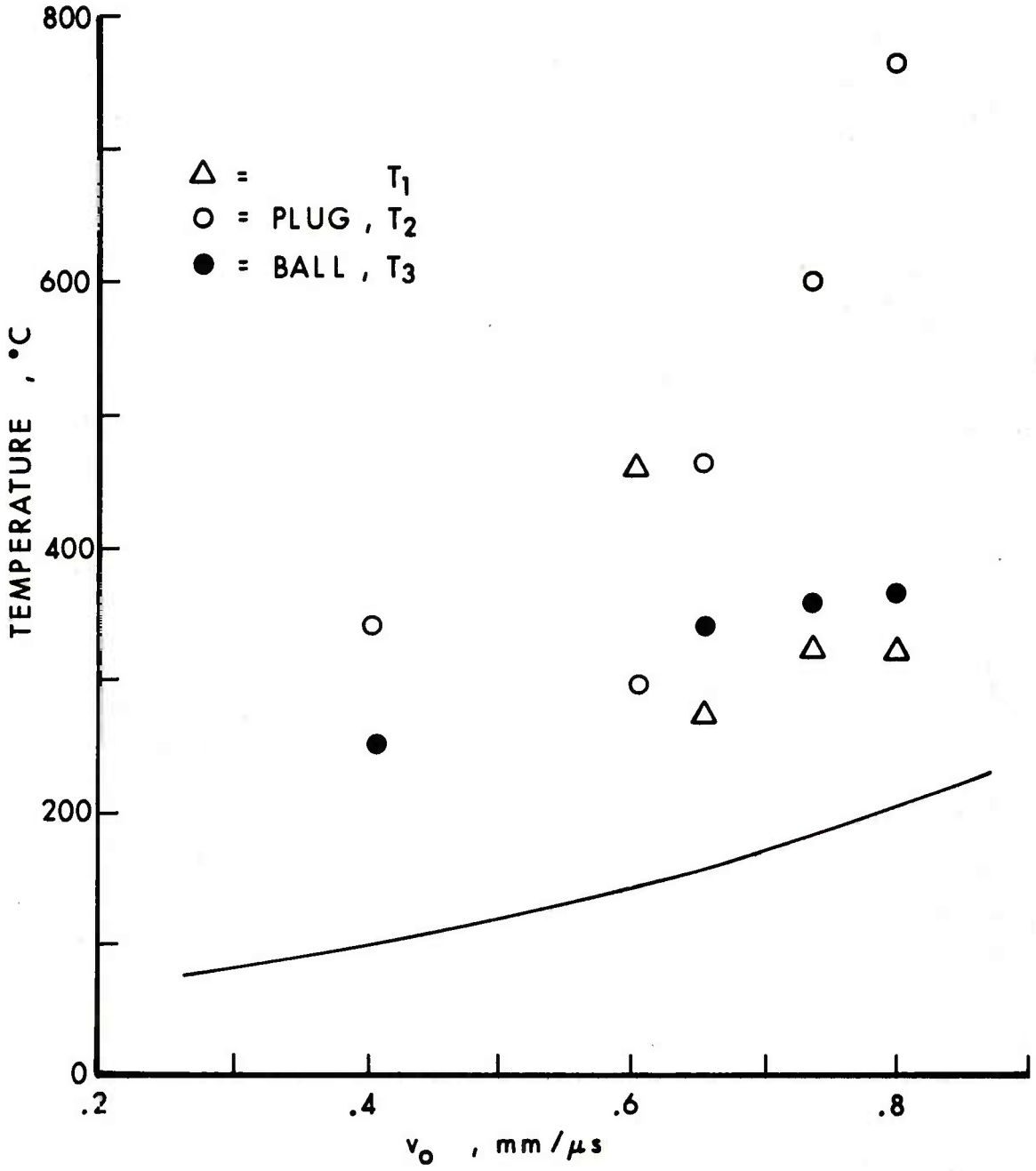

Figure 11. Plot of experimental data for the 3.2 mm targets. The points labeled T_1 exhibited a large increase in signal with impact velocity. The solid curve is the temperature predicted from the model.

Table IV. Projectile Temperature Data

Shot #	v_o (mm/μs)	T_1(°C)	T_2(°C)	Projectile (H=hard, A=annealed)	Trigger Position
880	0.756	-	200	A	31.8 mm
881	0.780	390	265	H	31.8 mm
883	1.22	370	-	A	85.7 mm
884	1.20	280	-	A	85.7 mm
886	1.23	390	-	A	41.3 mm
887	1.22	410	390		41.3 mm
SABOTED SPHERE PROJECTILES					
905	1.07	280	-	A	400. mm
906	1.22	220	275	A	400. mm
907	1.23	310	550	A	41.3 mm

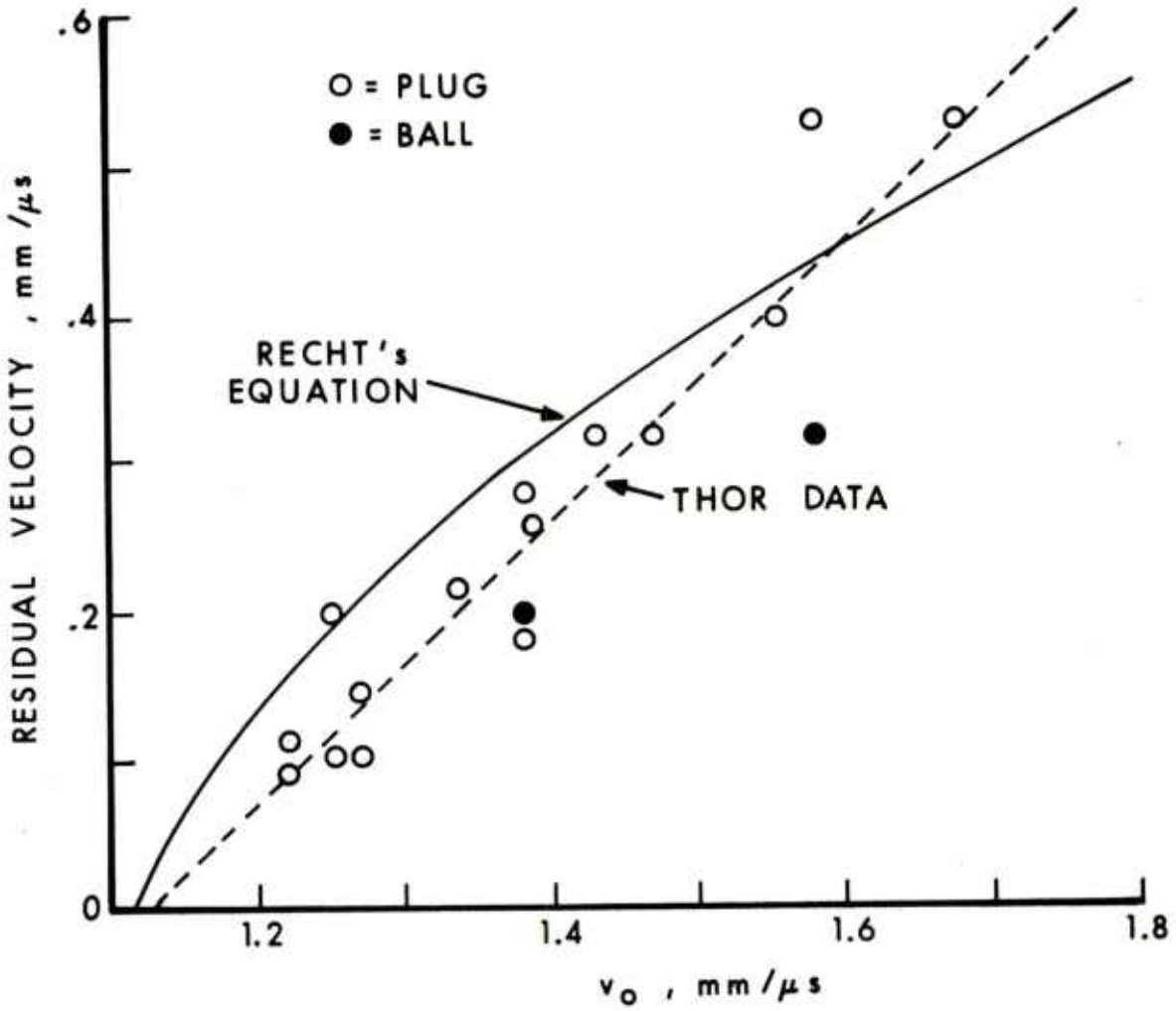

Figure 12. Experimental residual velocity versus impact velocity for the 12.7 mm targets as calculated from the radiometer records. The two curves are from empirical equations described in references 4 and 5.

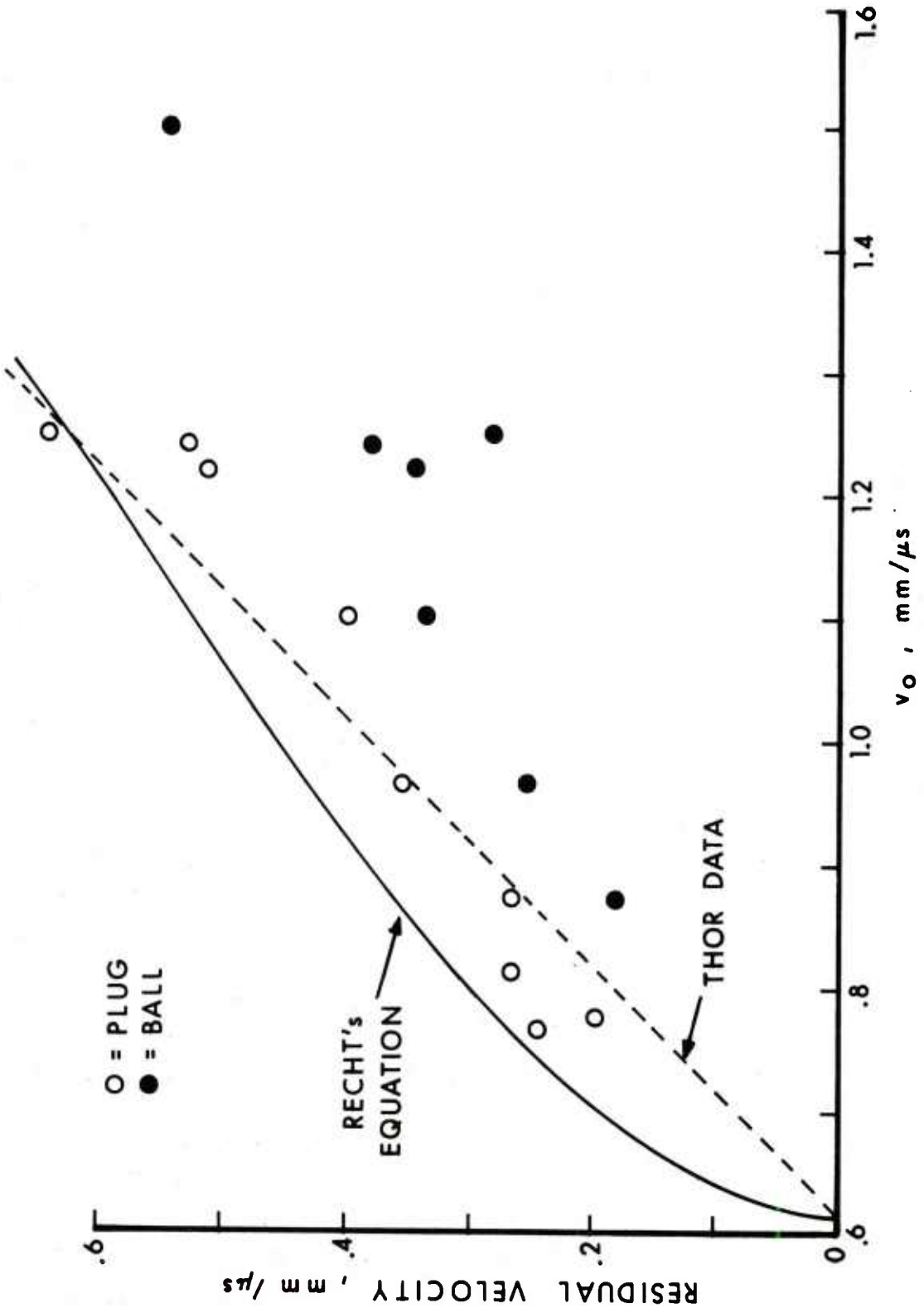

Figure 13. Experimental residual velocity versus impact velocity for the 6.3 mm targets as calculated from the radiometer records. The two curves are from empirical equations described in references 4 and 5.

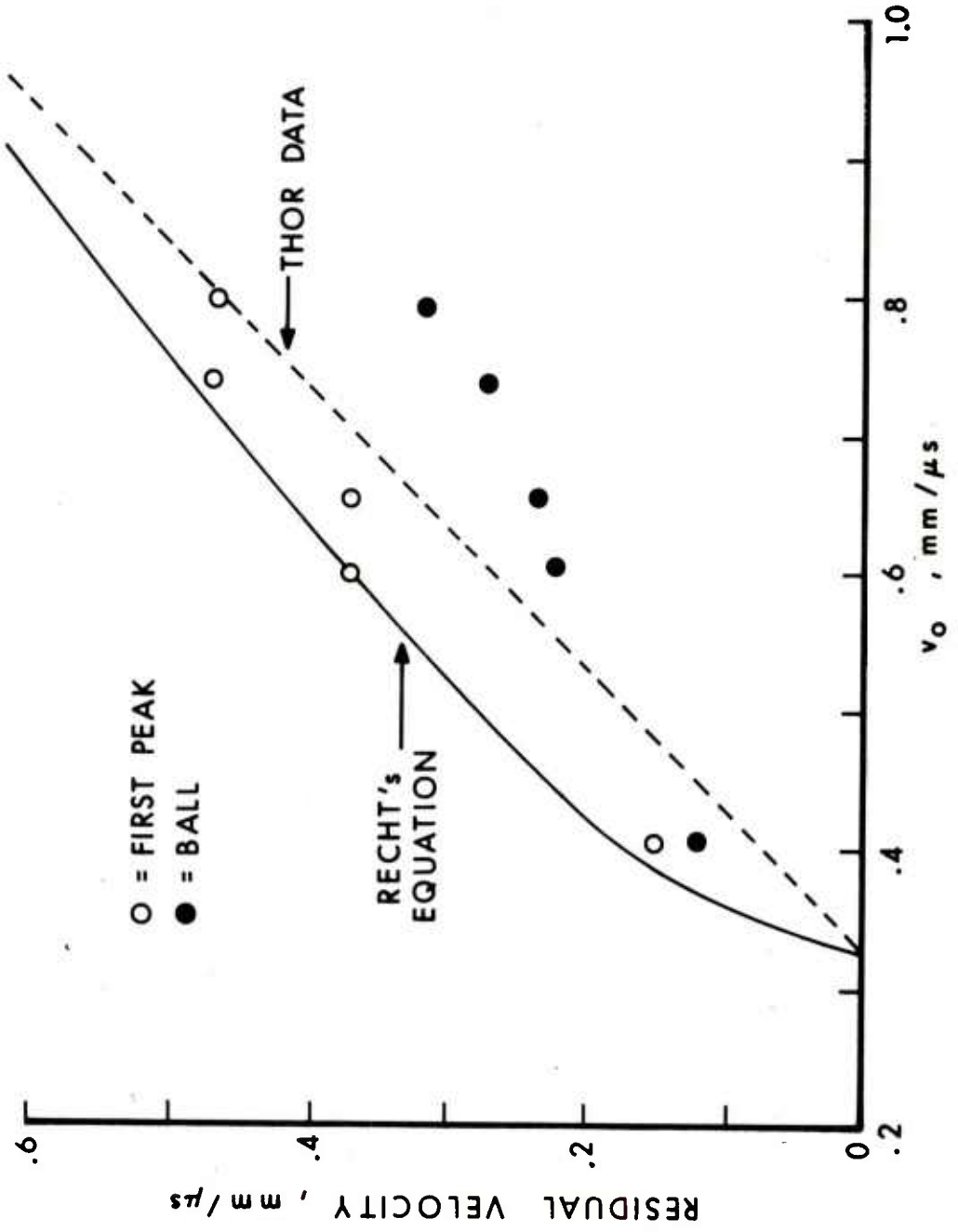

Figure 14. Experimental residual velocity versus impact velocity for the 3.2 mm targets as calculated from the radiometer records. The two curves are from empirical equations as described in references 4 and 5.

in Figures 12, 13 and 14 as smooth curves.

$$v_R = \frac{m_B}{m_B + m_p} \sqrt{\left(v_o^2 - v_{BL}^2\right)} \qquad (1)$$

m_B is the projectile mass; m_p the plug mass; v_o the impact velocity and v_{BL} the Ballistic limit velocity. v_{BL} was estimated from the formula for v_{BL} of the Thor data report[5]. v_{BL} is defined in that report as the velocity below which all attempts at perforation fail. The Thor data, derived from blunt-face projectiles, are also plotted as a function of impact velocity. The experimental data derived from the first radiance peak fall close to the smooth curves, but the velocities derived from the peaks assigned to the residual projectiles deviate systematically in each of the three cases. The assignments of the first peak to plug and the third to ball in the 6.3 mm and 3.2 mm cases thus seems reasonable. However, in the 3.2 mm case, the first peak may have been ejecta from the plate as was previously suggested. The assignment of peaks in the 3.2 mm experiments is uncertain. In the 12.7 mm case, the first two peaks are unresolved in most cases and the second observed peak is assigned to the ball. In the Thor experiments, the first fragment is the one measured, and it is possible that the ball should be somewhat slower. The fact that the experimental residual sphere data fall consistently below the Thor data for all three targets shows that our assignments of the residual sphere temperatures are at least consistent for all three targets.

IV. DISCUSSION

In order to compare the experimental results to calculated residual temperatures, the following simple model was formulated. If one assumes that the mechanical energy dissipated as heat by plastic work resides completely in the residual fragments and is uniformly divided, it is easily computed as follows.

$$\Delta E = \frac{1}{2} m_B v_o^2 - \frac{1}{2} (m_B + m_p) v_R^2 \qquad (2)$$

ΔE is the heat energy; the other symbols were introduced above. One

---

[5] *Ballistic Analysis Laboratory, Johns Hopkins University, "The Resistance of Various Metallic Materials to Perforation by Steel Fragments, Empirical Relationships for Fragment Residual Velocity and Weight," Project Thor Technical Report No. 41 (1969).*

then substitutes Recht's theoretical expression for residual velocity, equation (1), and derives an expression for the residual fragments (ball and plug combined) temperature rise, ΔT.

$$\Delta T = \frac{(\frac{1}{2} m_B - \frac{\frac{1}{2} m_B^2}{m_B + m_p}) v_o^2 + (\frac{\frac{1}{2} m_B^2}{m_B + m_p}) v_{BL}^2}{C (m_B + m_p)} \qquad (3)$$

C is the heat capacity for steel. Equation 3 is plotted in Figures 7, 9 and 11 as smooth curves. v_{BL} in each case was approximated by using the Thor Ballistic limit referred to above.

For the 12.7 mm case the experimental temperatures, which are mostly plug temperatures, all lie below the theoretical curve. In Figure 9, the 6.3 mm target results, the plug temperatures are distributed above and below the theoretical curve, and the assigned ball temperature points are mostly near the curve or below it. For the 3.2 mm target, Figure 11, all temperature points lie above the curve with the assigned plug temperatures well above and increasing rapidly with velocity.

This regular variation of experimental points from the theoretical values among the three target thicknesses can be interpreted as the failure of the simple assumption that the heat resulting from loss of mechanical energy elevates the plug and ball to the same temperature uniformly. There is too little time for heat conduction, and the ratio of ball mass to plug mass is quite different for the three targets considered. If one considers this non-uniformity, in the 12.7 mm case the ball should be relatively hotter and the plug cooler than predicted because the ball is considerably more distorted upon impact with the thick target than the target itself. At the other extreme, in the 3.2 mm case the ball is hardly distorted at all while the "plug" is wrapped around the ball. In the middle, the 6.3 mm case shows both ball and plug significantly distorted, and one expects both to be heated to the predicted values. Examination of the fragments of Figure 6 clearly shows the relative distortion. This seems to explain the relative position of the data with respect to the theoretical curves of Figures 7, 9 and 11.

Yet to be explained is the reason why the ball temperatures for the 3.2 mm targets lie above the values predicted on the basis of the simple model. The plug temperatures would be expected to be high and the ball temperature should be below the curve by the above argument. One obvious explanation is that the ball is never really observed because of its low temperature, and our assignment for this case is wrong. A more reasonable explanation is that the use of Recht's theoretical expression based on "plugging" is poorest for this thin-target case. These theoretical v_R's are large with respect to the impact velocities, as can be seen from Figure 14, and they yield unrealistically low values of the energy

dissipated given by equation (2). For the thicker targets the residual velocities are not as large compared with the impact velocities. Also, because of the greater contribution of the second term in equation (2) the effect of error in the value of v_{BL} will be relatively more important in the 3.2 mm case.

A refinement of the calculation using the smoothed experimental residual velocities may be more realistic but does not change the above argument concerning the relative amount of plastic work done on ball and plug. A much more detailed model would be required to include effects of non-uniform plastic work. As it is, even rough agreement of the experimental temperatures with the predictions of a simple, largely theoretical model is remarkable. The model as it is seems quite useful because of its conceptual simplicity and accuracy, and any further refinements would seem to be not worth the effort.

Since all of the measurements of this report were done in ambient air, the problem of air shock as a source of interference in the temperature measurements was considered. Most residual velocities in this study were below 0.5 mm/μs. If one computes the peak shock temperature for this velocity from the published Hugoniot of air,[6] assuming a particle velocity of 0.5 mm/μs, the result is 300°C. Also, the air shock is likely to be optically thin and not to contribute much to the observed radiances. Air shock was thus ignored except for the case of the projectile before impact.

V. CONCLUSIONS

The problem of temperature measurement of residual fragments from penetration was shown to be amenable to the two-color radiometric technique, which was introduced as a new tool for behind-the-target penetration diagnostics.

For the case of a steel sphere penetrating various thicknesses of mild steel, the data showed believable trends with impact velocity which came close to predictions of a simple model based on the loss of mechanical energy to plastic work heating.

A rather elaborate calculation[7] of the plastic work heating of 5 mm steel targets after impact with steel cylinders using the HELP code indicates essentially no dependence of temperature on impact velocity. However, direct comparison with the results of this report cannot be made since no experimental results were obtained for cylinders.

---

[6] *R. E. Shear and B. D. Day, "Tables of Thermodynamic and Shock Front Parameters for Air," BRL Report MR 1206, May 1959.* (AD #219224)

[7] *R. Frey, et al, "Initiation of Violent Reaction by Projectile Impact," Proceedings of the Sixth Symposium on Detonation, San Diego, California, August 1976.*

Future work on residual fragment temperature measurement could include an extension to different projectile shapes and various combinations of target materials. Also, it would seem that this experimental technique would be suitable for other systems where the transient nature of the effect or the rapid motion of the object precludes conventional measurement. An example of one study related to the work of this report would be the temperature measurement of explosively driven fragments to aid in the assessment of their lethality to explosives, propellants or other high energy systems.

ACKNOWLEDGMENT

The authors thank Dr. Philip Howe for posing the original problem which resulted in the successful completion of this work. A special thanks to J. J. Trimble for obtaining the calibration curves and other technical assistance.

REFERENCES

1. W. G. Von Holle and J. J. Trimble, "Residual Temperature of Shocked Solids by Two-Band Infrared Radiometry," BRL Report MR2624, May 1976. (AD #B011450L)
2. W. G. Von Holle and J. J. Trimble, "Temperature Measure of Shocked Copper Plates and Shaped Charge Jets by Two-Color I. R. Radiometry," J. Appl. Phys., 47, 2391, 1976.
3. W. G. Von Holle and J. J. Trimble, "Shaped Charge Temperature Measurement," Proceedings of the Sixth Symposium on Detonation, San Diego, California, August 1976.
4. R. F. Recht and T. W. Ipson, "Ballistic Perforation Dynamics," J. Appl. Mech., 30, 384, 1963.
5. Ballistic Analysis Laboratory, Johns Hopkins University, "The Resistance of Various Metallic Materials to Perforation by Steel Fragments, Empirical Relationships for Fragment Residual Velocity and Weight," Project Thor Technical Report No. 41, 1969.
6. R. E. Shear and B. D. Day, "Tables of Thermodynamic and Shock Front Parameters for Air," BRL Report MR1206, May 1959. (AD #219224)
7. R. Frey, et al, "Initiation of Violent Reaction by PRojectile Impact," Proceedings of the Sixth Symposium on Detonation, San Diego, California, August 1976.

DISTRIBUTION LIST

No. of Copies	Organization
12	Commander Defense Documentation Center ATTN: DDC-TCA Cameron Station Alexandria, VA 22314
1	Commander US Army Materiel Development and Readiness Command ATTN: DRCDMA-ST 5001 Eisenhower Avenue Alexandria, VA 22333
1	Commander US Army Aviation Systems Command ATTN: DRSAV-E 12th and Spruce Streets St. Louis, MO 63166
1	Director US Army Air Mobility Research and Development Laboratory Ames Research Center Moffett Field, CA 94035
1	Commander US Army Electronics Command ATTN: DRSEL-RD Fort Monmouth, NJ 07703
1	Commander US Army Missile Research and Development Command ATTN: DRDMI-R Redstone Arsenal, AL 35809
1	Commander US Army Tank Automotive Development Command ATTN: DRDTA-RWL Warren, MI 48090
2	Commander US Army Mobility Equipment Research & Development Command ATTN: Tech Docu Cen, Bldg. 315 DRDME-RZT Fort Belvoir, VA 22060
1	Commander US Army Armament Materiel Readiness Command Rock Island, IL 61202
1	Commander US Army Armament Research and Development Command ATTN: SARPA-FR-E, Dr. R. Walker Dover, NJ 07801
1	Commander US Army Harry Diamond Labs ATTN: DRXDO-TI 2800 Powder Mill Road Adelphi, MD 20783
1	Director US Army TRADOC Systems Analysis Activity ATTN: ATAA-SA White Sands Missile Range NM 88002
1	Chief of Naval Materiel Department of the Navy ATTN: MAT 03613, Dr. J. Amlie Washington, DC 20360
1	Commander US Naval Ship Research and Development Center ATTN: Mr. Harry Gray Carderock, MD 20034

DISTRIBUTION LIST

No. of Copies	Organization
1	Commander US Naval Surface Weapons Center ATTN: Mr. J. Logan Dahlgren, VA 22448
1	ASD/SE, Mr. Gaylord Oyler Wright-Patterson AFB, OH 45433
2	University of California Lawrence Livermore Laboratory Chemistry Department ATTN: Mr. H. Rizzo P. O. Box 808 Livermore, CA 94550

Aberdeen Proving Ground

Marine Corps Ln Ofc
Dir, USAMSAA